Heat Transfer Engineering, 26(8):41–49, 2005

ISSN: 0145-7632 print / 1521-0537 online
DOI: 10.1080/01457630591003754

Taylor & Francis
Taylor & Francis Group

Temperature Distribution in Different Materials Due to Short Pulse Laser Irradiation

ARINDAM BANERJEE, ANIL A. OGALE, CHAMPAK DAS, KUNAL MITRA, and CHELAKARA SUBRAMANIAN

Mechanical and Aerospace Engineering Department, Florida Institute of Technology, Melbourne, FL, USA

The purpose of this study is to analyze the heat-affected zone in materials such as meat samples, araldite resin-simulating tissue phantoms, and fiber composites irradiated using a mode-locked short pulse laser with a pulse width of 200 ps. The radial surface temperature profiles are compared with that of a continuous wave (CW) laser of the same average power. The short pulse laser results in a more localized heating than a continuous laser with a corresponding high peak temperature. A parametric study addressing the effect of pulse train frequency, material thickness, and amount of scatterers and absorbing agent in the medium and different initial sample temperatures is performed, and the measured temperature profiles are compared with the theoretical non-Fourier hyperbolic formulations and Fourier parabolic heat conduction formulations for both CW and pulsed laser cases.

INTRODUCTION

High-energy beams like x-rays and lasers, both continuous wave (CW) and pulsed, are being increasingly used in a variety of material processing, manufacturing, and biomedical applications. Traditionally, most laser applications in material processing and medicine involve using of a CW laser; more recently, though, short pulsed lasers are being used in a variety of applications such as remote sensing, optical tomography, laser surgery, and ablation processes. Pulsed lasers have the additional ability to control the width and depth of heating as well as induce high heating or cooling rates because of higher peak powers and shorter time duration [1].

The uses of short-pulsed lasers in medicine, with regard to diagnostics and therapy, has gained attention in the last decade. The advantages of using short-pulsed lasers rather than more traditional methods for surgical treatment include the precise control of the output energy of the device and the ability to control energy dissipation and the heat-affected zone. Thus, pulsed laser is used in a number of high-precision medical procedures like neurosurgery, ophthalmology, corneal surgery, and angioplasty [2–5]. Minimal damage to adjacent healthy tissues and efficient dosimetry are the surgical goals for these medical procedures. Minimally invasive techniques like Photodynamic Tumor Therapy (PDT) and Laser Interstitial Thermotherapy (LITT) have been developed over the years and are used effectively for the treatment of cancer or tumors [6–8]. Temperature rise and heat diffusion at the irradiated zone are two important parameters for these modes of therapy. In applications prior to tumor ablation, the temperature rise at the zone of treatment must be controlled effectively to ensure a total tumor cell necrosis at the desired location and also avoid carbonization of the surrounding healthy tissue [7]. With the advent of ultra-fast lasers, significant enhancements in damage localization over longer pulse durations have been attained [9]. The temperature fields in laser interstitial thermotherapy, localized hyperthermia, and other applications are directly related to the optical and thermal properties of the target tissues to determine a correct dosimetry for treatment [10]. The temperature field during ex vivo and in vivo laser interstitial thermotherapy has been modeled mathematically using an exponential decay model (Beer Lambert Law) and Fourier heat conduction equation. Effects of non-Fourier conduction on temperature distribution in laser-irradiated tissues have also been

The authors are thankful to Florida Solar Energy Center, Cocoa, Florida, for partial support of the project.

Address correspondence to Dr. Kunal Mitra, Mechanical and Aerospace Engineering Department, Florida Institute of Technology, 150 W. University Blvd., Melbourne, FL 32901. E-mail: kmitra@fit.edu

investigated theoretically using a hyperbolic heat conduction model [11].

With the advent of the pulsed laser, rapid advances are being made in material processing at submicron resolution length scales, termed laser micro machining [12]. Coupled with developments in nanotechnology and microelectromechanical systems (MEMS), laser micro machining is providing the user distinct advantages over other conventional machining processes [13]. The ability to control the temperature rise and minimize thermal damage in materials, the machinability of a greater range of applicable materials like metals and dielectrics, the precision machining capability, and the capability for sub-surface machining are some of the advantages it provides over conventional continuous wave heating [14–16]. Short-pulsed lasers are thus being used increasingly for micromachining, welding, etching, cutting, and a variety of material processing applications. Laser surface interaction is also of importance to applications involving thin film and coatings. Thermal characterization of materials, electronic components and modules represents a vital study to quantify and minimize the heat-affected zone during machining, fabrication, and testing of materials [17]. Numerical models to analyze the effects of laser fluence, radial beam variance, and laser power on materials having different thermal characteristic time have also been developed [18].

The current work gains much importance as it attempts a detailed experimental and theoretical analysis to characterize the nature of heat diffusion in different materials such as processed meat (bologna) samples, tissue phantoms, and fiber-composites using both CW and short pulsed lasers having pulse width of 200 ps. Temperature rise as a function of non-dimensional distance from the point of beam incidence for CW, short-pulsed heating of different samples, and the temporal temperature history of the samples are presented. The objective is to show that the heat-affected zone is significantly reduced by using a short-pulsed laser of the same average power as compared to a CW laser source. A parametric study involving the effect of pulse train frequency, material thickness, different amount of scatterers and absorbing dye, as well as different initial temperatures are undertaken. The experimental results are compared with theoretical models based on laser propagation through materials using hyperbolic and parabolic heat conduction equations [19, 20].

EXPERIMENTAL PROCEDURE

The schematic of the experimental setup is shown in Figure 1. A custom-built argon-ion mode-locked laser having a pulse width of about 200 ps (full width at half maximum) operating at a frequency of 76 MHz and a wavelength of 514 nm is used for the study. A Tellurium Dioxide crystal is used as a modulator in conjunction with a pulse generator (EH Research Lab, Inc.) to control the frequency of the pulse-train and the number of pulses irradiating the samples.

A thermal imaging camera (Thermovision 400 Series, AGEMA Infrared Systems) is used to record the surface temperature profile of the samples. The images are recorded with a National Instruments data acquisition system and processed with IMAQ Vision Builder Image processing software. The camera provides a measurement range of -4°F to 932°F with a sensitivity of $\pm 0.18^{\circ}$F at 86°F. The camera has an accuracy of $\pm 2\%$ in the measurement range. The time response of the camera is less than one second (the frequency at which data is recorded). The spectral response of the camera is 2 to 5 μm. When focused on the surface of the sample, the unit records the temperature profile. The camera uses a fixed lens ($25^{\circ} \times 25^{\circ}$) system, and the scanned field area at a distance of 0.4 m from the object is 0.15 m × 0.15 m. The image size is 640 pixels (H) × 480 pixels (V). For all experiments, the images are magnified twice (using the MAG 2 feature in the camera). Thus, the lowest spatial resolution that can be obtained at this setting is 0.117 mm (H) × 0.156 mm (V). The object distance is maintained at 0.4 m for all experiments. The laser beam diameter (d_{beam}, as in Figure 2) is found to be 2 mm by taking an image of the laser incident on a piece of paper. The pixel intensity profile is measured in two mutually perpendicular directions, and the $1/e^2$ length is evaluated. Thus, it can be seen that the beam spot is considerably larger than the camera interrogation spot. When the

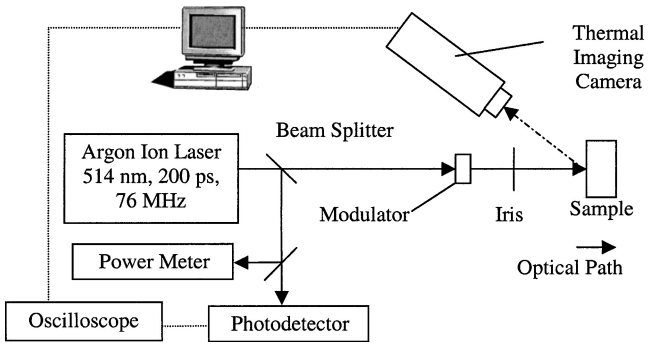

Figure 1 Schematic of the experimental setup.

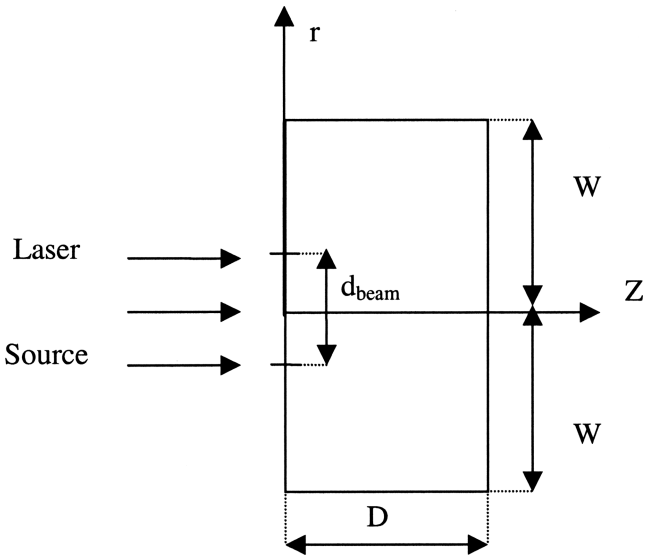

Figure 2 Schematic of the coordinate system used for analysis.

sample is then scanned in the radial direction, it is made sure that the spatial averaging does not include any temperatures of colder material outside the irradiated region. As seen in Figure 1, the thermal imaging camera is placed at an angle relative to the optical axis of the laser beam. It is generally expected that the emissivity will have directional properties based on the angle of vision and type of material being irradiated. Experiments are performed on samples by varying the angle in increments of 10°. The variations in temperature are found within the uncertainty of the measurement. Thus, the emission is assumed to be isotropic for all measurements. The laser power is continuously measured with a power meter (Model #1830 C, Newport Corporation). The pulse width is monitored using an ultra-fast photo-detector (Model # 1454, New Focus, Inc.) and displayed on an oscilloscope with fast time-resolved modules (Tektronix 7854).

Different samples used in this study are processed meat, tissue phantoms, and fiber composites. The processed meat (bologna) samples available in any grocery store are in the shape of finite cylinders of approximately 5.4 cm radius. Two different thicknesses of the meat, 4 mm (0.15 inches) and 8 mm (0.30 inches), are used for the study. The fiber composites used for analysis are 4 mm (0.15 inches) in thickness and are in square shapes of sides 2.5 cm (1 inch). Tissue-simulating phantoms composed of araldite, DDSA (Dodecenyl Succinic Anhydride), and DMP-30 (hardener) are casted in the laboratory. DDSA is mixed with the resin for polymerization, and the hardener is added to catalyze the reaction. The three constituents are mixed in the ratio 1:0.87:0.04. Titanium Dioxide particles (mean diameter: 0.3 μm) are added as scatterers to the sample. The scattering coefficients are estimated based on the number density of scatterers per gram of resin used. Samples are cast having scattering coefficients of 3.5 mm^{-1} and 7 mm^{-1}, following the principle as outlined in the literature [21]. Water-based red dye having high absorptivity in the spectral region 500–550 nm are also added to the samples. The absorption coefficients are based on the volume of dye added to the sample per gram of resin. Sample absorption coefficients of 0.1 mm^{-1} and 0.05 mm^{-1} are used in the study. The tissue phantoms used for the analysis are cast in square shapes of sides 2.5 cm (1 inch) and thicknesses 4 mm (0.15 inches) and 8 mm (0.30 inches). After mixing the scatterers and absorber dye with the resin matrix, the samples are cured in the oven for 36 hours (Energy Beam Sciences, MA). The vinyl foam composite used has been made from epoxy resin and two layers of fiber glass on the top and bottom of the vinyl foam. The samples are well insulated on all sides (except on the irradiated face) to prevent heat loss to the surroundings.

Controlling the on–off time of the modulator by the pulse generator varies the number of pulses per train. The average power for each setting is noted separately, and continuous wave heating is performed at the same average power. The effect of pulse train frequency is also studied by controlling the repetition rate (2.5 kHz, 10 kHz, and 100 kHz) of the pulse train irradiating the sample. The number of pulses irradiating the sample is kept constant in all three cases. All of the runs are repeated without insulating the samples. To study the effect of initial sample temperature, all of the studies are performed for three different initial sample temperatures: 68°F, 55°F, and 45°F. The samples that needed to be cooled for establishing different initial temperatures are refrigerated along with the insulation to eliminate any thermal inertia effects at the beginning of the experiment.

One limitation of the thermal imaging camera is that it can be used only to record the surface temperature history of the sample. To study the propagation of heat within the medium, thermocouples are inserted radially into the tissue phantoms using a hollow steel guide. High thermal conductivity grease is applied at the interface of the thermocouple and the sample to eliminate the effect of thermal contact resistance. The thermocouples used are copper-constantan (T-type) having a wire diameter of 0.254 mm (0.01 in.). All thermocouples are connected to a computerized data acquisition system.

A statistical uncertainty analysis is conducted using data from multiple runs. Though each experiment is conducted a minimum of three times, the data are reported for only one because the deviation (0.5°F) between different runs is found to be insignificant and the experiments are easily repeatable. The camera is calibrated to a known temperature before the experiments, thereby eliminating a bias error. Considering a 95% confidence level, a value of precision index is evaluated at each data point. Because the bias error is eliminated by calibration, the overall uncertainty is taken to be the precision index evaluated at each data point.

THEORY

Thermal analysis of laser-material interaction in various applications is usually conducted via the traditional parabolic Fourier conduction model [22]. The Fourier model implies that the speed of propagation of the thermal signal is infinite, such that the effect of a perturbation in the temperature at any point in the medium is instantaneously felt at every location in the material, even if the intervening distances are very large. The hyperbolic model accounts for the time required for the heat flux to relax or adjust to a change in the temperature gradient. If the speed of propagation of the thermal signal is considered finite via a hyperbolic conduction formulation, the temperature profiles will be significantly different than those predicted by the classical Fourier models, particularly during the initial transients and regions close to the surface of the medium [11, 23, 24]. In order to compare the experimentally measured temperature profiles, a non-Fourier damped wave model for the case of laser penetration and absorption of the intensity within the material is considered for analysis [11, 25]:

$$q(r,z,t) + \tau \frac{\partial q(r,z,t)}{\partial t} = -\kappa \nabla T(r,z,t) \tag{1}$$

$$-\nabla q(r,z,t) + k_a L(r,z,t) = \rho C \frac{\partial T(r,z,t)}{\partial t} \tag{2}$$

where q is the heat flux, r and z are the spatial co-ordinates, T is the temperature, t is the time, κ is the thermal conductivity, τ is the thermal relaxation time, k_a is the absorption coefficient, ρ is the density, L is the laser intensity (heat flux), and C is the specific heat. The case under consideration is a pulsed laser beam that is incident normally on a sample, as shown in Figure 2. The beam is Gaussian in radial direction, and therefore an axi-symmetric cylindrical co-ordinate system is chosen to describe the geometry. The laser intensity (heat flux) distribution is given by:

$$L(r, z, t) = L_0 \exp\left(-\frac{2r^2}{\sigma^2}\right) \exp(-zk_a) g(t) \tag{3}$$

where L_0 is the peak laser intensity and σ is the spot radius. The temporal distribution of the pulse train $g(t)$ is approximated as a rectangular profile [25] and given by:

$$g(t) = [H(t) - H(t - t_p)] \tag{4}$$

where $H(t)$ is a unit step function. Eqs. (1) to (4) can be combined for the two-dimensional axi-symmetric cylindrical co-ordinate systems as follows:

$$\frac{\partial^2 T}{\partial r^2} + \frac{1}{r}\frac{\partial T}{\partial r} + \frac{\partial^2 T}{\partial z^2} = \frac{1}{\alpha}\frac{\partial T}{\partial t} + \frac{\tau}{\alpha}\frac{\partial^2 T}{\partial t^2} - \{(1 + \delta(t)) - (1 + \delta(t - t_p)\} \times \frac{L_0 k_a}{\kappa} \exp\left(-\frac{2r^2}{\sigma^2}\right) \exp(-zk_a), \tag{5}$$

where α is the thermal diffusivity and $\delta(t)$ is the delta function. Equation (5) yields a finite wave speed ($= \sqrt{\alpha/\tau}$) for the propagation speed of the thermal wave. In the limit $\tau \to 0$, Eq. (5) becomes the parabolic Fourier heat conduction equation. The boundary conditions are selected to simulate the experimental conditions. All of the boundaries except the incident laser irradiated face are insulated.

RESULTS

Equations (1) to (5) are solved numerically by using an Alternating Direction Implicit (ADI) scheme [26]. The thermophysical properties used in the numerical simulation are given in Table 1. The meat bologna samples used in this paper are exactly identical to the ones used previously [19]. A detailed description about the determination of thermophysical parameters and thermal relaxation time can be found in previous work [19]. The numerical solutions are obtained by using values of Δz and Δr as 4.0×10^{-4} m and Δt as 0.01 seconds for the CW case and 25×10^{-12} seconds for the pulsed case. Reducing the grid size by one order of magnitude, which correspondingly increases the number of nodes, checks the stability, and the results are found to be convergent. The pulse train frequency of 10 kHz is used unless otherwise mentioned. The rise in temperature of the sample is plotted numerically as a function of non-dimensional distance, which is obtained by normalizing the radial distance by the half-width of the sample. It must be mentioned here that the default temperature setting in the IR camera is in English units, which is commonly used by the medical community and various processing industries; thus, all temperatures are reported in °F.

Experiments are conducted with insulated meat samples for CW and pulsed laser irradiation for the same average power of 150 mW. The results are then compared with the numerical results for a Fourier parabolic and a non-Fourier hyperbolic heat conduction formulation for 10 seconds. With a 95% confidence interval, the precision index for a total of three runs for the test case is 4.303. The standard deviation between the three runs at each individual nodal point along the surface is evaluated. The bias error of the camera is removed by calibration. Thus, the total uncertainty values at each nodal point is the product of the precision index multiplied by the standard deviation. It can be seen in the CW case that a maximum total uncertainty of 1.15°F is obtained at a location 0.045 from the center, while for the pulsed case, the maximum uncertainty 1.51°F is obtained at a location 0.01 from the center.

The experimental results are found to be in good agreement with the non-Fourier case, as is evident from Figures 3 and 4. This can be attributed to the fact that the non-Fourier hyperbolic model is more suitable for laser heating of tissue samples, as it takes into account the time required for the heat flux to

Table 1 Thermo-physical properties of processed meat (bologna) samples from literature [19]

Property	Value	Units
Thermal conductivity, κ	0.80 ± 0.04	W/m.K
Density, ρ	1230 ± 10	kg/m^3
Specific heat, C	4.66 ± 0.20	kJ/kg.K
Thermal diffusivity, α	$1.40 \times 10^{-7} \pm 0.12 \times 10^{-7}$	m^2/s
Absorption coefficient, k_a	0.4 ± 0.05	cm^{-1}
Relaxation time, τ	5	seconds

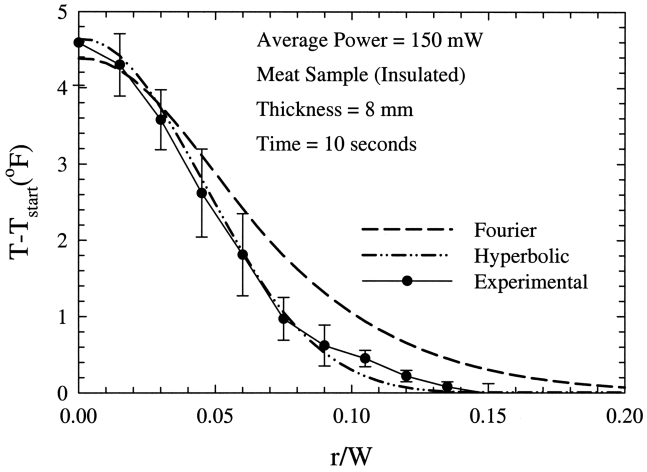

Figure 3 Comparison of experimental measurements with Fourier and hyperbolic numerical modeling results for a CW laser heating.

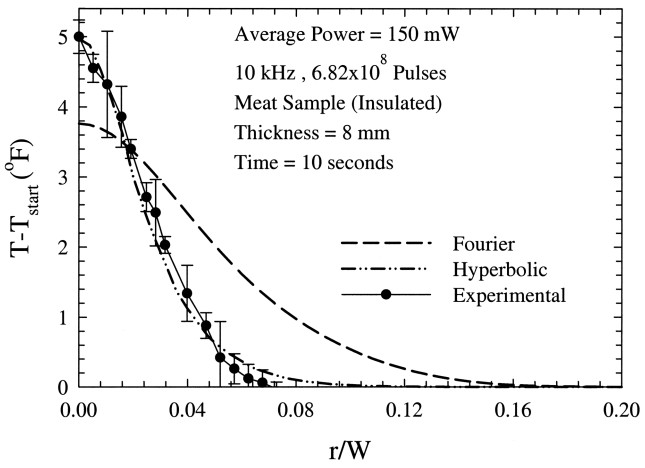

Figure 4 Comparison of experimental measurements with Fourier and hyperbolic numerical modeling results for a pulsed laser heating.

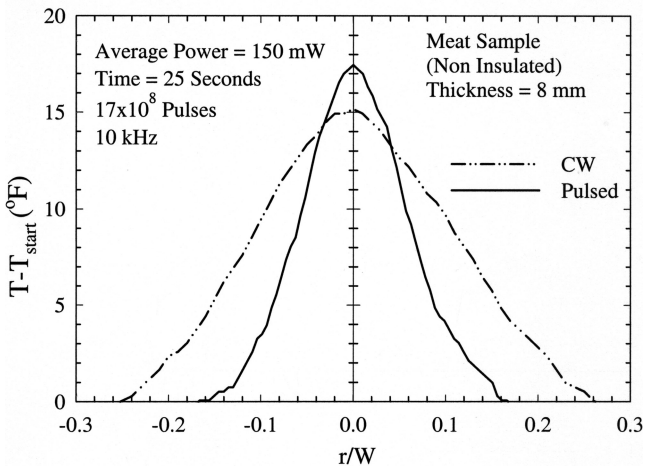

Figure 6 Comparison of surface temperature distribution for a non-insulated meat sample.

relax or adjust to a change in temperature gradient. The traditional Fourier model, which takes into consideration an infinite speed of propagation, indicates that a local change in temperature causes an instantaneous perturbation.

In order to clearly demonstrate the difference between pulsed and CW laser heating, experimental results for an 8 mm-thick sample are plotted in Figure 5. The sample is insulated from the surroundings. It is observed that when the sample is irradiated with a pulsed laser beam, the peak temperature reached at the surface is higher than that attained with a corresponding CW heating. Less energy is spread along the radial direction as compared to a CW irradiation; thus more localized heating with a higher peak temperature is observed at the surface, as seen in Figure 5.

Experiments are also conducted without the insulation, as shown in Figure 6. As observed in Figure 6, the heat-affected zone and the rise in temperature are found to be less than an insulated sample under the same conditions. The presence of insulation prevents heat loss by dissipation to the surroundings from all surfaces. Experiments are also repeated with different initial temperatures for both the insulated and non-insulated case. Wide ranges of initial temperatures are tested, but only three temperatures (68°F, 55°F, and 45°F) are reported in this study. For the range of experiments performed, it is observed that the radial distribution and rise in temperature do not depend on the initial temperature of the samples.

The effect of variation in tissue phantom thickness is shown in Figure 7. A higher peak temperature and a corresponding lower radial spread are observed for the 8 mm sample as compared to a 4 mm sample. An increase in thickness causes more volumetric energy absorption, resulting in a higher peak temperature at the irradiated surface. As the input laser energy is same for both cases, the sample with a greater thickness exhibits a corresponding lesser radial spread. This conclusion is based on the volumetric energy absorption model for hyperbolic heat transfer. The model is in sharp contrast to the surface absorption model, where an increase in thickness results in an immediate increase in the surface temperature. The volume penetration

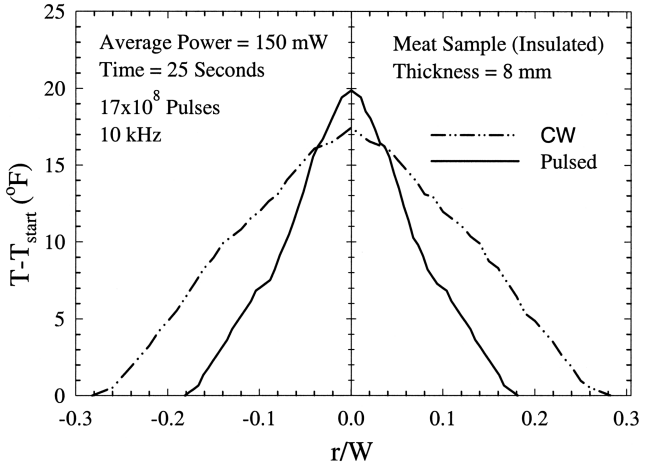

Figure 5 Comparison of surface temperature distribution for an insulated meat sample.

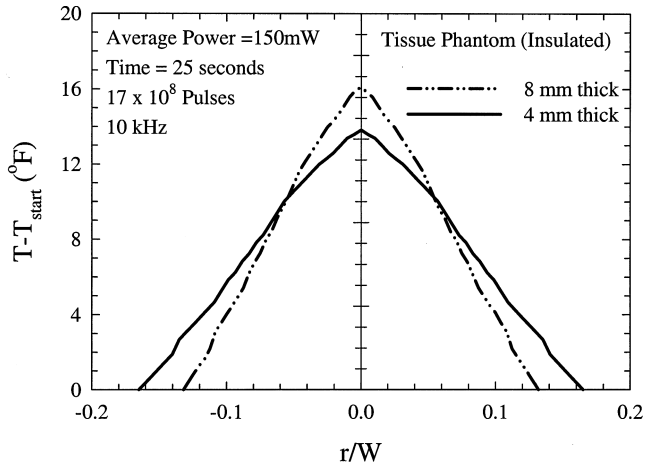

Figure 7 Comparison of surface temperature distribution for a different tissue phantom thickness.

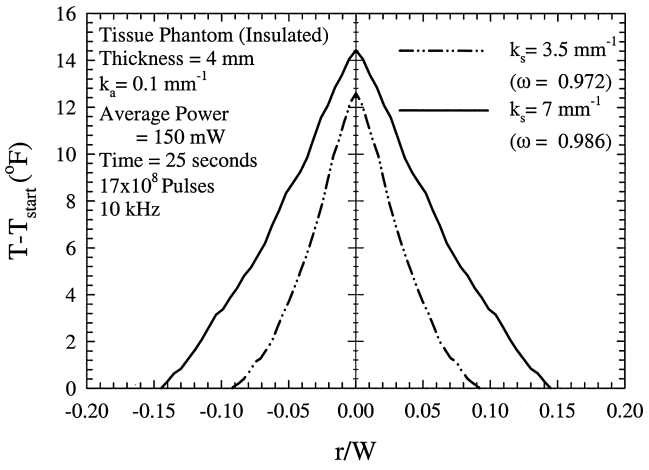

Figure 8 Effects of varying scattering coefficients on temperature distribution in a tissue phantom.

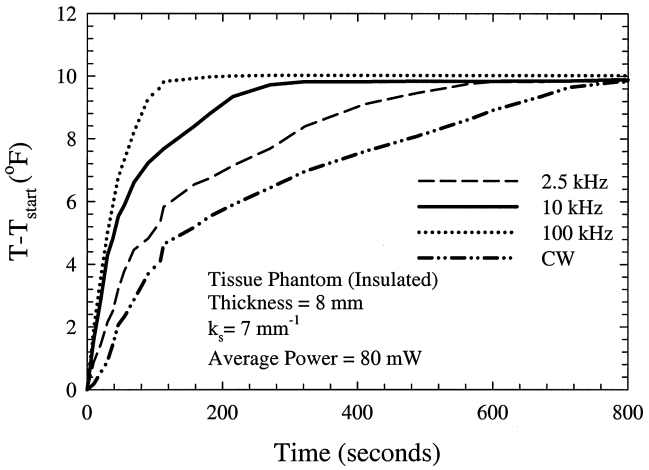

Figure 10 Effect of pulse train frequency on surface temperature for a tissue phantom.

assumes that more heat is absorbed inside the sample with an increase of thickness that results in a lower surface temperature.

The scattering coefficient (k_s) of the sample is also found to have an effect on the temperature distribution. The higher the amount of titanium dioxide in the sample, the more the scattering coefficient leads to a wider radial temperature spread and a higher peak value. This is observed in Figure 8. The absorption coefficient is kept constant for the above case. Experiments are also conducted with samples having different absorption coefficients but the same scattering coefficient, as illustrated in Figure 9. It is observed that with an increase in the absorption coefficient, more energy is absorbed inside the medium leading to a lower surface temperature. The conclusion is based again on the volumetric energy absorption model, and a similar conclusion can be made about increase of absorption coefficient of the sample as that of the increase of thickness. However, for both cases, it is seen that with an increase in the scattering albedo ($\omega = k_s/(k_s + k_a)$), the radial surface temperature increases.

The effect of pulse train repetition rate is studied by varying the pulse train frequency (2.5 kHz, 10 kHz, 100 kHz). The total number of pulses and the average power of the laser are kept constant for all the above cases. It is observed from Figure 10 that as the pulse frequency is decreased, the material requires more time to attain the same peak temperature. A lower frequency means a larger time lag between two successive pulses irradiating the sample, resulting in a longer time to attain the peak temperature. The results are then compared with a CW case of the same average power. CW implies continuous heating, but the corresponding peak power is less than that of the pulsed cases, resulting in a lower temperature rise. The time taken to reach a steady-state value is also longer for the CW case, as is evident in Figure 10.

Figure 11 shows a temporal history for different samples: fiber composites, meat, and tissue phantoms. The laser average power, number of pulses/unit time, and repetition rate are all kept constant for the three cases. It is observed that the fiber composite shows a higher surface temperature and lower thermal conductivity as compared to the meat and the phantoms. A lesser amount of energy is propagated into the medium, resulting in a higher surface temperature. The thermal conductivity of the phantoms is higher than that of meat, resulting in more

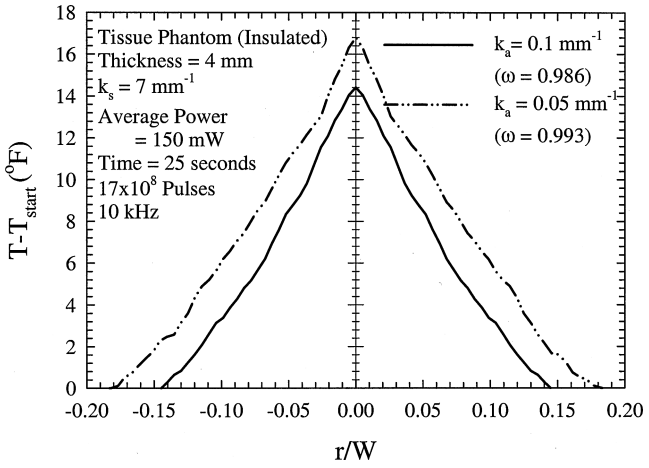

Figure 9 Effects of varying absorption coefficients on temperature distribution in a tissue phantom.

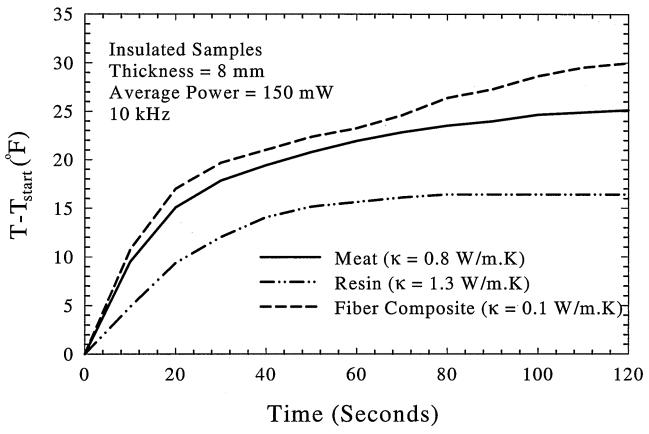

Figure 11 Surface temperature distribution for different materials of the same thickness.

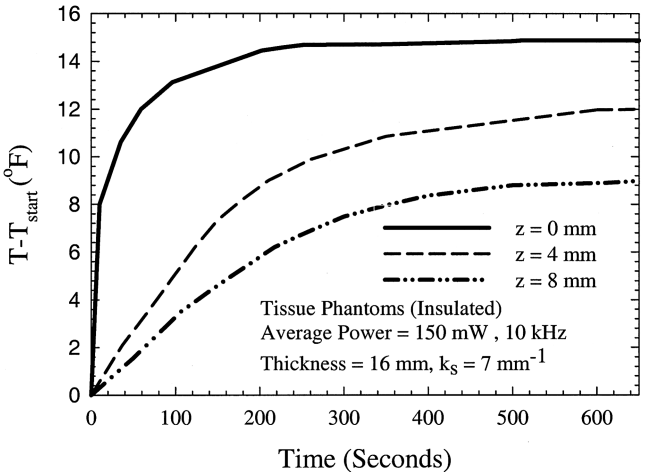

Figure 12 Temperature history at different locations of a tissue phantom.

heat propagation and a corresponding lower radial temperature distribution.

Experiments are also conducted with a short-pulsed laser by inserting thermocouples inside the tissue phantoms. Thermocouples are inserted at locations 4 mm and 8 mm from the sample surface. The temperature history for the surface and different thermocouple locations are plotted in Figure 12. The temperature plot for $z = 0$ (i.e. the irradiated surface of the sample is measured with the thermal imaging camera). The plot shows that even at large times, thermal equilibrium of the tissue phantoms is not attained. This could have implications in laser surgery, where the depth of the affected area is of importance after a finite time.

The effect of variation of pulse width in laser irradiation of materials is also studied numerically for better understanding this phenomenon. Three different laser pulse widths are considered for numerical computations: 200 ps, 20 ps, and 2 ps. The results are plotted in Figure 13. It is observed that as the pulse width decreases, a lesser radial spread accompanies the rise in surface temperature. This can be attributed to the fact that with a shorter laser pulse width, the instantaneous energy source irradiating the sample is higher, leading to a greater rise in surface temperature. Thus, short-pulsed lasers in the picosecond scales can be used more effectively for laser surgery or laser material processing applications where damage to surrounding areas needs to be minimized.

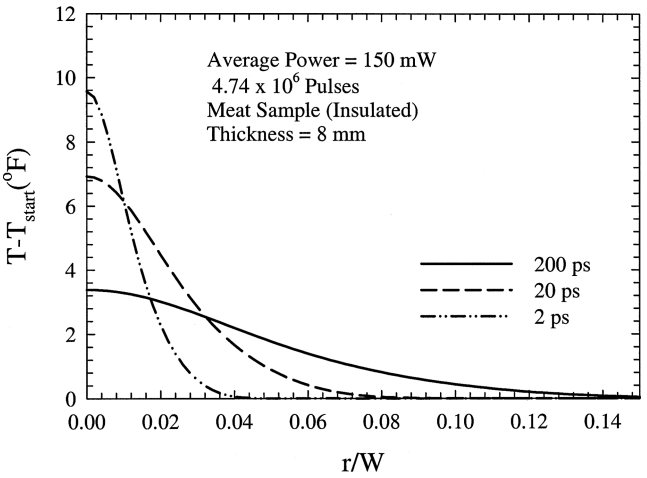

Figure 13 Numerical simulation showing the effect of variation of pulse width.

CONCLUSION

The experiments performed demonstrate the claim that short-pulsed laser heating results in a lower heat-affected region compared to a CW source and is thereby suitable for applications where minimal damage to the surroundings is of importance. The temperature rise for the case of short-pulsed laser heating is much higher than heating with a CW laser source of the same average power. It is observed that the temperature rise and surface temperature distribution are functions of the thickness of the sample and amount of scatterers and absorbers in the medium. Initial sample temperature plays no role in the temperature distribution of the medium.

The results also demonstrate that the theoretical non-Fourier hyperbolic heat conduction equation is a better approximation than the traditional parabolic Fourier heat conduction formulation for modeling the temperature distribution in tissues due to both short-pulsed and CW laser irradiation. The results of this research have a tremendous impact on bioheat transfer and lay the foundation for development of tools to analyze further work for heat and mass transfer in biological systems. The results are also of importance to machining and fabrication applications, where the heat-affected zone is critical for material performance.

NOMENCLATURE

C	specific heat
D	thickness of sample
$g(t)$	temporal distribution of pulse train
$H(t)$	unit step function
k_a	absorption coefficient
k_s	scattering coefficient
L	laser source term
L_0	maximum intensity of the laser beam
q	heat flux
r	radial co-ordinates
t	time
t_p	laser pulse width
T	temperature
W	half-length of the sample
z	axial co-ordinates

Greek Symbols

α	thermal diffusivity
$\delta(t)$	delta function

κ	thermal conductivity
ρ	density
σ	spot radius of the laser beam
τ	thermal relaxation time
ω	scattering albedo
∇	gradient

REFERENCES

[1] Tien, C. L., and Qiu, T. Q., Heat Transfer Mechanisms during Short-Pulse Laser Heating of Metals, *Journal of Heat Transfer*, vol. 115, pp. 835–841, 1993.

[2] Spooner, G. J. R., Juhasz, T. T., Imola, R., Djotyan, G., Horvath, C., Sacks, Z., Marre, G., Miller, D., Williams, A. R., and Kurtz, R., New Developments in Ophthalmic Applications of Ultra Fast Laser Source, *Proc. SPIE—Commercial and Biomedical Application of Ultrafast Lasers II*, San Jose, CA, vol. 3934, pp. 62–70, January 2000.

[3] Marion, J. E. II, and Kim, B.-M., Medical Applications of Ultra-Short Pulse Lasers, *Proc. of SPIE—The International Society for Optical Engineering*, Proceedings of the 1999 Commercial and Biomedical Applications of Ultrafast Lasers, San Jose, CA, USA, vol. 3616, pp. 42–50, January 1999.

[4] Loesel, F. H., Tien, A.-C., Backus, S., Kapteyn, H., Murnane, M., Kurtz, R. M., Sayegh, S., and Juhasz, T., Effect of Reduction of Laser Pulse Width from 100 ps to 20 fs on the Plasma-Mediated Ablation of Hard and Soft Tissue, *Proc. SPIE—The International Society for Optical Engineering*, Proceedings of the 1998 Thermal Therapy, Laser Welding, and Tissue Interaction, Stockholm, Sweden, vol. 3565, pp. 116–123, September 1998.

[5] Kurtz, R. M., Elner, V., Liu, X., Juhasz, T., Loesel, F. H., Horvath, C., Niemz, M. H., and Noack, F., Plasma-Mediated Ablation of Biological Tissue with Picosecond and Femtosecond Laser Pulses, *Proc. SPIE—Laser-Tissue Interaction VIII,* San Jose, CA, vol. 2975, pp. 192–200, February, 1997.

[6] Milne, P. J., Parel, J. M., Manns, F., Denham, D. B., Gonzalez-Cirre, X., and Robinson, D. S., Development of Stereo-tactically Guided Laser Interstitial Thermotherapy of Breast Cancer: In Situ Measurement and Analysis of the Temperature Field in *Ex Vivo* and *In Vivo* Adipose Tissue, *Lasers in Surgery and Medicine*, vol. 26, pp. 67–75, 2000.

[7] Manns, F., Milne, P. J., Gonzalez-Cirre, X., Denham, D. B., Parel, J. M., and Robinson, D. S., In-Situ Temperature Measurements with Thermocouple Probes during Laser Interstitial Thermometry (LITT): Quantification and Correction of a Measurement Artifact, *Lasers in Surgery and Medicine*, vol. 23, pp. 94–103, 1998.

[8] Svanberg, S., New Developments in Laser Medicine, *Physica Scripta,* vol. T72, pp. 69–75, 1997.

[9] Zysset, B., Fujimoto, J. G., and Deutsch, T. F., Time-resolved Measurements of Picosecond Optical Breakdown, *Applied Physics B: Photophysics and Laser Chemistry*, vol. 48, no. 2, pp. 139–147, 1989.

[10] Newman, W. H., Lele, P. P., and Bowman, H. F., Tissue Thermal Property Measurements during Microwave and Ultrasound Hyperthermia: A Caveat, *Collected Papers in Heat Transfer: Winter Annual Meeting of the ASME*, Chicago, IL, vol. 103, pp. 45–50, 1988.

[11] Vedavarz, A., Mitra, K., and Kumar, S., Hyperbolic Temperature Profiles for Laser Surface Interactions, *Journal of Applied Physics*, vol. 76, no. 9, pp. 5014–5021, 1994.

[12] Liu, X., Du, D., and Tai, Y. C., Laser Ablation and Micro-Machining with Ultrashort Laser Pulses, *IEEE Journal of Quantum Electronics*, vol. 33, no. 10, pp. 1706–1716, 1997.

[13] Gower, M., Excimer Laser Micro-Fabrication and Micromachining, *SPIE—The International Society for Optical Engineering*, First International Symposium on Laser Precision Micro-fabrication, Omiya, Japan, vol. 4088, pp. 124–131, June 2000.

[14] Mao, S. S., Greif, R., Mao, X., and Russo, R. E., Plasma Development during Picosecond Laser Processing of Electronic Materials, *ASME Journal of Heat Transfer*, vol. 122, p. 424, 2000.

[15] Shirk, M. D., and Molian, P. A., A Review of Ultrashort Pulsed Laser Ablation of Materials, *Journal of Laser Applications*, vol. 10, no. 1, pp. 18–28, 1998.

[16] Asheghi, M., Touzelbaev, M. N., Goodson, K. E., Leung, Y. K., and Wong, S. S., Temperature-dependent Thermal Conductivity of Single-Crystal Silicon Layers in SOI Substrates, *Journal of Heat Transfer*, vol. 120, no. 1, pp. 30–36, 1998.

[17] Kolzer, J., Oesterschulze, E., and Deboy, G., Thermal Imaging and Measurement Techniques for Electronic Materials and Devices, *Microelectronic Engineering*, Elseveir Science, vol. 31, pp. 251–270, 1996.

[18] Mitra, K., Kumar, S., and Vedavarz, A., Parametric Aspects of Electron-Phonon Temperature Model for Short Pulse Laser Interactions with Thin Metallic Films, *Journal of Applied Physics*, vol. 80, no. 2, pp. 675–680, 1996.

[19] Mitra, K., Kumar, S., Vedavarz, A., and Moallemi, M. K., Experimental Evidence of Hyperbolic Heat Conduction in Processed Meat, *Journal of Heat Transfer*, vol. 117, pp. 568–573, 1995.

[20] Vedavarz, A., Mitra, K., Kumar, S., and Moallemi, M. K., Effect of Hyperbolic Conduction on Temperature Distribution in Laser Irradiated Tissue with Blood Perfusion, *ASME Winter Annual Meeting, Advances in Biological Heat and Mass Transfer*, HTD-vol. 231, pp. 7–16, 1992.

[21] Arridge, S. R., Cope, M., and Delpy, D. T., The Theoretical Basis for the Determination of Optical Path Lengths in Tissue: Temporal and Frequency Analysis, *Physics in Medicine and Biology*, vol. 37, no. 7, pp. 1531–1560, 1992.

[22] Martin, G. T., and Bowman, H. F., The Temperature Distribution in Laser Irradiated Tissue with Blood Perfusion, *National Heat Transfer Conference*, ed. H. R. Jacobs, Houston, TX, vol. 96, pp. 97–102, 1998.

[23] Tzou, D. Y., *Macro- to Microscale Heat Transfer*, Taylor and Francis, Washington, DC, 1997.

[24] Ozisik, M. N., and Tzou, D. Y., On the Wave Theory in Heat Conduction, *Journal of Heat Transfer*, vol. 116, pp. 526–535, 1994.

[25] Hector, L. G., Kim, W.-S., and Ozisik, M. N., Hyperbolic Heat Conduction Due to a Mode Locked Laser Pulse Train, *International Journal of Engineering Science*, vol. 30, no. 12, pp. 1731–1744, 1992.

[26] Anderson, D. A., Tannehill, J. C., and Pletcher, R. A., *Computational Fluid Mechanics and Heat Transfer*, 2nd ed., Taylor and Francis, Philadelphia, PA, pp. 139–142, 1997.

Arindam Banerjee received his Master of Science degree in Mechanical Engineering from the Florida Institute of Technology, Melbourne, Florida, in 2002, and his B.S. from Jadavpur University, Calcutta, India, in 1999. His main research interests are lasers and their applications in fluids, material processing, and biomedical field; microscale fluidics; and heat transfer. He is currently pursuing his Ph.D. at Texas A&M University, College Station, Texas.

Anil A. Ogale received his Master's degree from the Florida Institute of Technology, Melbourne, Florida, in 2002. His research interests are lasers and their applications for biomedical and remote sensing fields, and control systems for manufacturing process. Currently he is a Ph.D. student at the University of Washington, Seattle, at the Polymer Optics and Processing Laboratory.

Champak Das received his Master of Science degree in Mechanical Engineering from the Florida Institute of Technology, Melbourne, Florida, in 2003, and his B.S. from Jadavpur University, Calcutta, India, in 1998. His main research interests are laser based diagnostics and microfluidics. He is currently completing his Ph.D. at the University of Florida.

Kunal Mitra is an Associate Professor in Thermal Science area at the Florida Institute of Technology, Melbourne, Florida. He received his Ph.D. in 1996 from Polytechnic University, Brooklyn, NY. His main research interests are lasers and their applications in material processing and biomedical field, thermal radiation transport modeling and experiments, microscale heat transfer, and energy systems. He has published more than fifty articles in well-recognized journals, books, and conference proceedings.

Chelakara S. Subramanian is a Professor of Mechanical and Aerospace Engineering in Experimental Fluid Mechanics area at the Florida Institute of Technology, Melbourne, Florida. He received his doctorate from the University of Newcastle, Australia, in 1982. His main research interests include temperature- and pressure-sensitive paints, short-pulse laser detection of thermal tile debonding, gas turbine blade film cooling, and turbulence structure of highly roughened boundary layers. He has over 65 technical publications in international journals, books, and proceedings, and a patent to his credit.